Rigorous Analysis of Mode Propagation and Field Scattering in Silicon-Based Coplanar MIS Slow Wave Structures with Abrupt Transitions to Transmission Lines on Normal Substrate

Shuoqi Chen, Rüdiger Vahldieck, *Senior Member, IEEE,* and Jifu Huang

Abstract— **This paper presents a rigorous field theoretical analysis of slow wave mode propagation in coplanar waveguide (CPW) metal-insulator-semiconductor (MIS) transmission lines with a laterally confined doping profile. Two types of transmission line structures are investigated—bulk silicon and semiconductor-on-insulator (SOI). In both cases a Gaussian profile of the doping depth is assumed. It was found that an optimum lateral width of the doping region exists for which both structures exhibit a much better slow wave factor at lower losses than traditional thin-film MIS transmission lines. The abrupt transition between MIS, CPW, and CPW on a normal insulating substrate was investigated as well. It was found that the reflection coefficient increases significantly with frequency and when the lateral width of the doping region is extended over the whole cross section of the CPW. The investigation was carried out using the frequency-domain transmission line modeling (TLM) (FDTLM) method.**

I. Introduction

IT IS well known that metal–insulator–semiconductor MIS transmission lines support slow wave mode propagation. This phenomenon, combined with the attractive features of coplanar waveguide (CPW), are of increasing interest in the design of monolithic microwave-integrated circuits (MMIC) for wireless communications systems in the 1–2 GHz range and for high-speed digital integrated circuits. However, slow wave mode propagation in semiconductor-based transmission lines comes at the price of relatively high losses and low Q-factors, which are problems that have prevented the widespread use of metal-insulator-semiconductor (MIS) CPW in the past. This problem has been studied experimentally and theoretically by several researchers [1]–[7], and it was found that thin-film MIS CPW are in general less lossy than thick-film structures [6], [9], but that the latter can sustain slow wave mode propagation over a wider frequency range than the former. A compromise between a maximum slow wave factor and minimum losses can be found either by carefully controlling the doping-layer thickness or by limiting the lateral width of the doping region. The latter approach was investigated by Wu and Vahldieck [8], [9] for thick and thin-film MIS CPW. By gradually lowering the doping level in a lateral direction with maximum doping below the center conductor, it was found that losses can be reduced significantly, and at the same time a moderate slow wave factor can be maintained. Although this approach is generally helpful in improving the Q-factor of a MIS CPW, its practical realization is difficult with epitaxial technology. A better approach is to keep the doping level constant within a laterally confined region. The lateral width of the doping region must then be optimized for a maximum slow wave factor and minimum losses.

In the following, this problem is investigated in more detail with special consideration for the physical process of realizing MIS CPW. As it is well known, ion-implantation into a semiconductor is easily achieved through a mask window. However, this results in an abrupt transition between the doped and the undoped region. Applied to a thin-film MIS CPW, the lateral doping profile changes abruptly rather than gradually (Fig. 1). To achieve the same or better slow wave characteristics as those obtained by the gradual doping profile, an optimum lateral width of the doping region must be found. To investigate the effect of different lateral doping widths on the slow wave characteristics, we have considered two different structures—bulk silicon and semiconductor-on-insulator (SOI). In both cases the p^+-doping layer is realized by implanting boron ions (B^{2+}) through the photoresist-mask window, whereby the size of the window determines the lateral width of the doping region. The added difficulty in this investigation is due to the fact that the doping level changes with penetration depth into the semiconductor and shows a Gaussian-like doping depth profile.

Since the MIS CPW with a lateral doping confinement still exhibits considerable losses, the length of a transmission line with a doped region (in the propagation direction of the wave) should be kept to a minimum. This leads inevitably to an abrupt transition between the doped and undoped substrates

Manuscript received March 28, 1996. This work was supported in part by the National Science and Engineering Research Council of Canada (NSERC) and by a GREAT Award from the Science Council of British Columbia, Canada.

S. Chen and R. Vahldieck are with the Department of Electrical and Computer Engineering and the Laboratory for Lightwave Electronics, Microwaves and Communications (LLiMiC), University of Victoria, Victoria, B.C., V8W 3P6, Canada.

J. Huang is with the Department de Genie Electrique et de Genie Informatique, Ecole Polytechnique de Montreal, C.P. 6079, Montreal, H3C 3A7, Canada.

Publisher Item Identifier S 0018-9480(96)08525-0.

(Figs. 5 and 6) and, thus, introduces additional losses. This problem has not been discussed in the literature yet, but is very important when slow wave structures are integrated with other circuit parts. To quantify these losses we have calculated for the first time the scattering parameters for such a transition. First, we considered only the transition from an undoped to a doped substrate of a limited lateral extent and no step in the metal conductor in order to isolate the scattering effect of the doped substrate from that of the metal discontinuity. Secondly, we also included steps in the conductor widths of the CPW.

To calculate the electromagnetic field in transmission line cross-sections of this kind is very difficult because the doping distribution is inhomogeneous in the lateral and vertical directions. While the lateral width of the doping region depends only on the dimensions of the photoresist mask, the vertical doping-level depth depends on the doping process and shows approximately a Gaussian-like profile for which the distribution can be found from the LSS range theory for amorphous targets (the unified theory of atomic stopping by Lindhard, Scharff, and Schiott) [10]. Once the doping-depth profile is known, the frequency-domain transmission line matrix (FDTLM) method [11]–[16] is applied to compute the slow wave factor, the corresponding losses, and the scattering matrix of the transitions. The advantages of the FDTLM method have been discussed in previous papers and only a brief description of the method will be given here. The structures investigated in the following underline once more the flexibility of this approach.

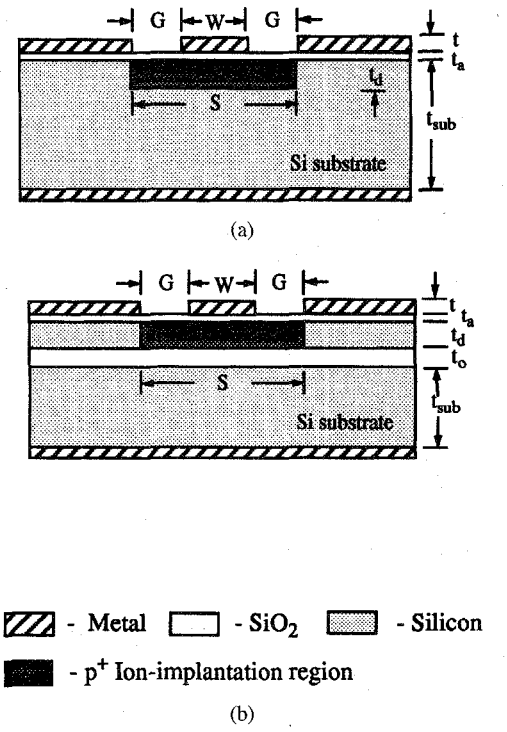

Fig. 1. Cross sections of two types of MIS coplanar waveguides. (a) Bulk silicon and (b) SOI. The doping region is obtained by Boron dopant ion-implantation at energy levels of 200 keV.

II. Method of Analysis

A. Slow Wave Mode Propagation

The geometrical layout of the two types of coplanar MIS structures investigated in this paper is presented in Fig. 1(a) and 1(b), respectively. The first step in the analysis is to model the conductivity distribution in the doping layer. Once this is accomplished, the cross section of the structure is discretized by frequency-domain nodes. Each of these nodes represents the electromagnetic field at that location under the influence of the local material parameters. The FDTLM algorithm then governs the interaction of the electromagnetic field in between the nodes. Details of this approach will be discussed briefly. First, however, we outline the approach of how to determine the material parameters.

Both structures in Fig. 1 consist of a thin p^+-doping region separated from the conductor layer by a thin insulating layer of SiO_2. The structure in Fig. 1(b) contains an additional insulating layer of SiO_2 between the p^+ layer and the bulk silicon. This structure is also referred to as SOI. While in conventional MIS CPW the semiconductor is doped homogeneously over the entire cross section of the structure, we limit the doping range in the lateral direction to the area below the center conductor and the two slots, because this is the area in which the electric field of the fundamental mode is most prominent. The p^+-doping region is fabricated by B^{2+} implantation into the silicon substrate. According to the LSS range theory, the implanted B^{2+} concentration in silicon is approximately a Gaussian distribution function of depth, which may be expressed as

$$N(x) = \frac{D}{\sqrt{2\pi}\,\Delta Rp} \exp\left[-(x - Rp)^2/\Delta Rp^2\right] \qquad (1)$$

where D is the total number of ions implanted per unit area, x is the distance measured along the axis of incidence, $N(x)$ is the density of the implanted B^{2+} that stop at the plane x, Rp is the projected range which estimates the depth at which the concentration of implanted dopants reaches its maximum value, and ΔRp is the average fluctuation in the projected range. After taking account of diffusion effects that may occur during implantation or during the annealing treatment, Fig. 2 illustrates the relative-conductivity depth profile of the very thin p^+-doping region (about 2-μm thickness) in the silicon substrate. The parameters of both MIS CPW structures in Fig. 1 are:

$W = 40\ \mu$m, $G = 25\ \mu$m;
SiO_2 layer $t_a = 1000$ Å, $\epsilon_r = 3.9$, $\sigma = 0$;
Doping region $t_d = 2.0\ \mu$m; $\sigma = 30.6 \sim 0.5$ S/mm;
SOI structure $t_d = 1\ \mu$m, $\epsilon_r = 11.8$,
ρ (SOI resistivity) $= 10\ \Omega$-cm,
$t_o = 2\ \mu$m;
Si substrate $t_{\text{sub}} = 525\ \mu$m, $\epsilon_r = 11.8$,
ρ (Si substrate resistivity) $= 20\ \Omega$-cm.

The conductivity depth profile shown in Fig. 2 determines the material parameters at the location of the FDTLM nodes. The FDTLM algorithm then models the interaction of the electromagnetic field among the nodes. The nodes utilized

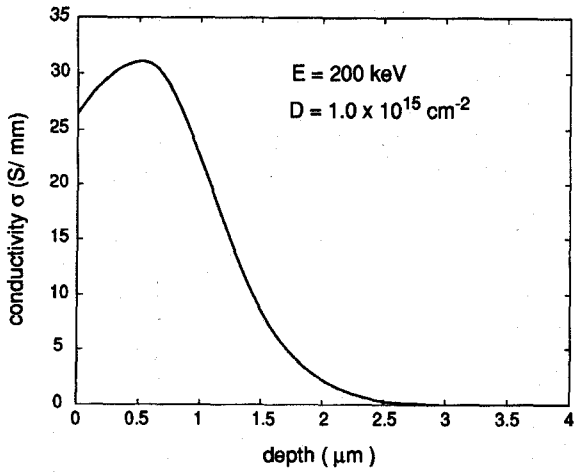

Fig. 2. The conductivity profile in silicon obtained by Boron ion-implantation with doses of 1×10^{15} B^{2+} ions/cm^2 at energy levels of 200 keV (after annealing).

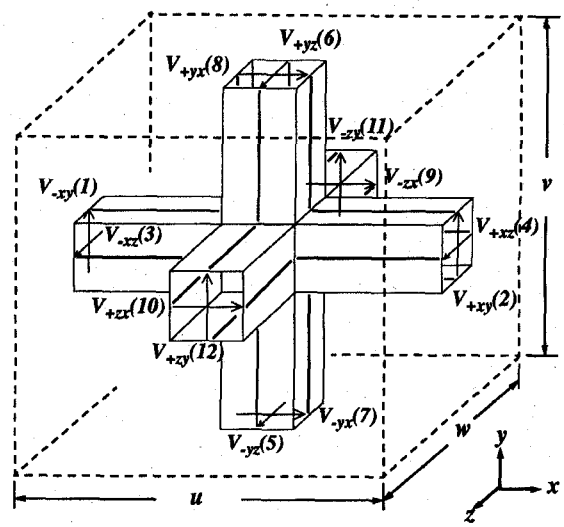

Fig. 3. The symmetrical condensed FDTLM node.

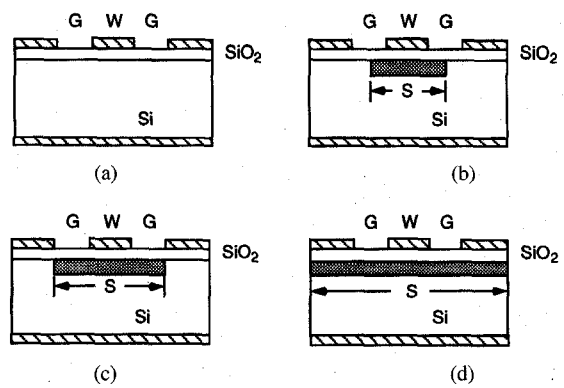

Fig. 4. Bulk silicon and SOI MIS CPW with (a) an undoped ($S = 0$) and (b), (c), (d) three different lateral doping structures (b) $S = W + 2(G/2)$; (c) $S = W + 2G$; (d) over entire cross section.

in the FDTLM method are mostly based on the symmetrical condensed node (SCN) shown in Fig. 3. Other nodes are possible and are described in numerous publications. The interaction between the transmission lines of the SCN are given by the scattering matrix at the node center. In contrast to the time-domain TLM (TDTLM) method [17], [18], in which an impulse excitation leads to a time-iterative procedure of scattering at each node and interconnection with its neighboring nodes, the FDTLM algorithm works entirely in the frequency domain. That is, the FDTLM network is considered to be in a steady-state where scattering and interconnection occurs simultaneously. The advantage of this approach is that time synchronism (required in the TDTLM) is not needed and that a graded mesh layout with a large grading ratio can be chosen. This is particularly useful in the present analysis because of the very thin inhomogeneous substrate-layers that are in close proximity to larger structural details. In the network of TLM nodes used to discretize the transmission line network, the electromagnetic field is represented by voltages and currents on the node link lines. The network is characterized by the intrinsic scattering matrix, S_{ism}, which represents all the internal branches of a network by the network branches pointing in the propagation direction of the wave [12]. For a two-dimensional (2-D) propagation problem this has the advantage that the guided wave structure can be considered as a periodic network with periodicity of Δz in the propagation direction. Based on Floquet's theorem the periodic structure can be reduced to a single unit cell, and the intrinsic scattering matrix S_{ism} is constructed from one slice of the waveguide which contains only as many FDTLM SCN's as needed to discretize the cross section of the structure. The propagation constant γ and its corresponding eigenvectors (voltages) can be determined by solving the following eigenvalue equation [12], [16]:

$$\cosh(\gamma \Delta z) \cdot V = A \cdot V \tag{2}$$

where V is the vector containing voltages at the exterior branches of the waveguide slice (the cross-section of the waveguide), and Δz is the length of the slice (the SCN's dimension along the propagation direction). Matrix A is found from the S_{ism} of the waveguide slice [12], [16]. Equation (2) yields the transverse-electromagnetic field distribution and the propagation constants γ of the propagating modes supported by the structure at a given frequency.

B. Scattering Parameters of the Slow Wave MIS CPW Discontinuity

Integrating the slow wave structures of Figs. 4(c) and (d) into other circuit parts results in an abrupt transition between the undoped and the doped silicon as depicted in Fig. 5. Furthermore, since a given characteristic impedance on the conductor dimensions in the slow wave region is different from the undoped region, steps in the conductor width must also be considered. This is illustrated in Fig. 6.

The FDTLM method has been applied in the past to characterize CPW discontinuities on a lossless substrate, and good agreement with other techniques and measurements was found [11]–[16]. The present problem is more challenging due to the fact that now location-dependent lossy material parameters have to be accounted for in the FDTLM nodes. The S-parameter extraction technique developed for the FDTLM

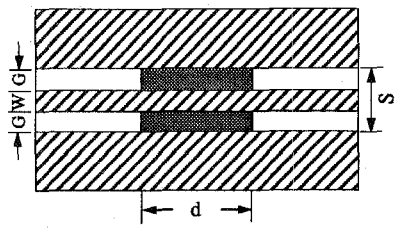

Fig. 5. Top view of an abrupt discontinuity between an undoped CPW on high-resistivity silicon and an MIS CPW with a laterally confined doping region ($S = W + 2G$).

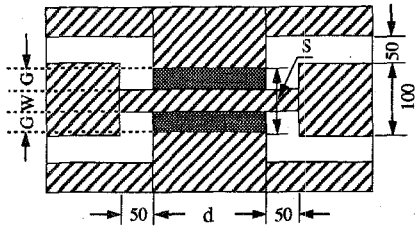

Fig. 6. Top view of a double-step discontinuity between an undoped CPW on high-resistivity silicon and MIS CPW (top view) with a laterally confined doping region ($S = W + 2G$).

method remains the same as in previous papers (i.e., [12]) and is briefly discussed in the following. The MIS CPW section can be considered as a discontinuity region attached to two CPW transmission lines as input and output ports. The intrinsic scattering matrices for the discontinuity region and the two attached semi-infinite CPW transmission lines are determined from a 2-D analysis. They are denoted by S_M, S_{R1}, and S_{R2}, respectively. The incident and reflected waves at the interfaces to the discontinuity region and the attached CPW transmission lines are related as follows:

$$\begin{bmatrix} b_1 \\ b_2 \end{bmatrix} = S_M \cdot \begin{bmatrix} a_1 \\ a_2 \end{bmatrix} = \begin{bmatrix} S_{M11} & S_{M12} \\ S_{M21} & S_{M22} \end{bmatrix} \cdot \begin{bmatrix} a_1 \\ a_2 \end{bmatrix} \tag{3}$$

where a_1, b_1 are the incident and reflected waves at the interface of the left CPW transmission line and the discontinuity region, while a_2, b_2 are the incident and reflected waves at the interface of the right CPW transmission line and the discontinuity region. The system is then excited by injecting the mode-field distribution of the fundamental mode of the left CPW (known from an eigenvalue analysis of that transmission line) at the left interface. The reflected and transmitted waves at the discontinuity region are then obtained from:

$$a_2 = S_{R2} \cdot b_2 \tag{4}$$

$$b_2 = T \cdot a_1 = T \cdot (S_{R1} \cdot b_1' + a_{10}) \tag{5}$$

where the reflected and transmitted waves contain all modes (including propagating and evanescent modes) of the corresponding CPW transmission lines. The modal field coefficients of a specific mode can be extracted by using

$$[A] = [a_i]^{-1} \cdot a \tag{6}$$

$$[A] = [b_i]^{-1} \cdot b. \tag{7}$$

In order to obtain the scattering parameters, the modal fields a_i and b_i are normalized to 1W of power and the scattering parameters of the first mode at the input and output ports are found as

$$S_{11} = A_1^r = [a_i]^{-1}\big|_{i=1} \cdot a_1 \tag{8}$$

$$S_{21} = A_1^t = [b_i]^{-1}\big|_{i=1} \cdot b_1 \tag{9}$$

where A_1^r and A_1^t are the first elements of (6) and (7) with a substituted by the first element of the total reflected and transmitted waves from which the final scattering parameters can be calculated [16].

III. Numerical Results and Discussions

A. Slow Wave Propagation in MIS CPW

The structures of the MIS CPW lines investigated in the following are shown in Fig. 1. They are made from bulk silicon [Fig. 1(a)] or SOI [Fig. 1(b)]. For both structures the doping-depth profile is assumed to be Gaussian. Four different lateral doping-widths have been investigated as shown in Fig. 4 a) $S = 0$; (b) $S = W + 2^*(G/2)$; (c) $S = W + 2^*G$; and (d) $S =$ doping over the entire CPW cross section. For faster computation, the metallization thickness is assumed to be zero, and metallic losses have not been considered. Fig. 7 illustrates the propagation constant, loss factor, and Q-factor of the bulk silicon MIS CPW for the different lateral doping-widths of Fig. 4. Fig. 8 shows the corresponding results for the SOI MIS CPW. To verify the results, a comparison with the method of lines [8] is included. For both structures it was found that the configuration in Fig. 4(c) shows the lowest-loss slow wave mode propagating over the frequency range between 0.7–5.0 GHz. The highest slow wave factor, however, can only be obtained from the structure in Fig. 4(d).

1) The Bulk Silicon MIS CPW: Fig. 7(a) and (b) illustrate that a compromise exists between the maximum slow wave factor and minimum losses. For the structure in Fig. 4(c) the maximum attenuation is less than 0.75 dB/mm at 5 GHz and less than 0.3 dB/mm at 2 GHz. At the same time the slowing factors λ_0/λ_g are between 12.5–13 with very little dispersion over the frequency range of 0.7–5.0 GHz. This slowing factor corresponds to effective dielectric constants of 156.3–169.0, which are much larger than the dielectric constant of either the Si substrate or the SiO_2 insulating layer. The losses found with the structure in Fig. 4(c) are less than the data reported in literature [3]–[9] for structures with homogeneous doping over the entire transmission line cross section. Also the quality factor, Q, shown in Fig. 7(c), reaches a higher value compared to the much larger MIS CPW structures on GaAs [1] or other microstructure CPW MIS transmission lines [4]. The numerical results for the structure in Fig. 4(b) are verified by measurements and shown in Fig. 7. This good agreement indicates that the other numerical results are also a true picture of the physical reality.

2) The SOI MIS CPW: Similar characteristics can be observed for the SOI structure shown in Fig. 8. In comparison with the silicon bulk structure, the slow wave factor is generally approximately 15% higher and shows somewhat less dispersion. At the same time the attenuation is only 3.5%

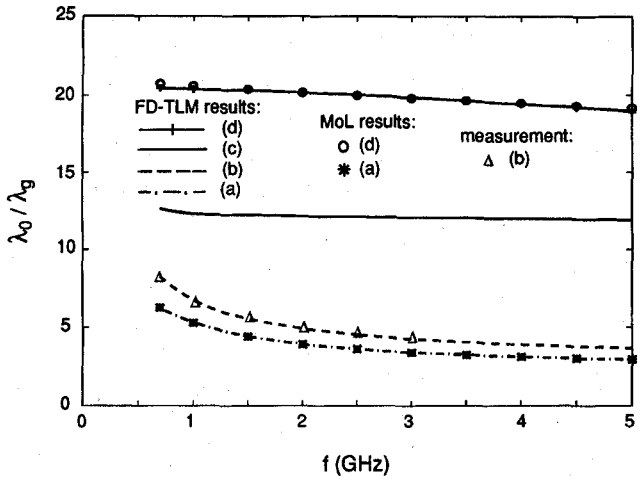

(a)

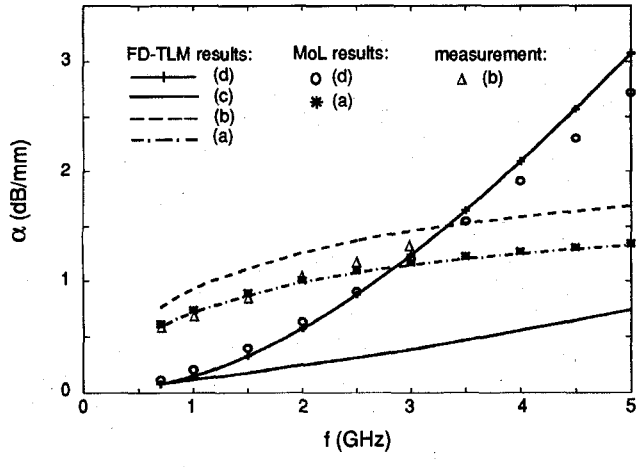

(b)

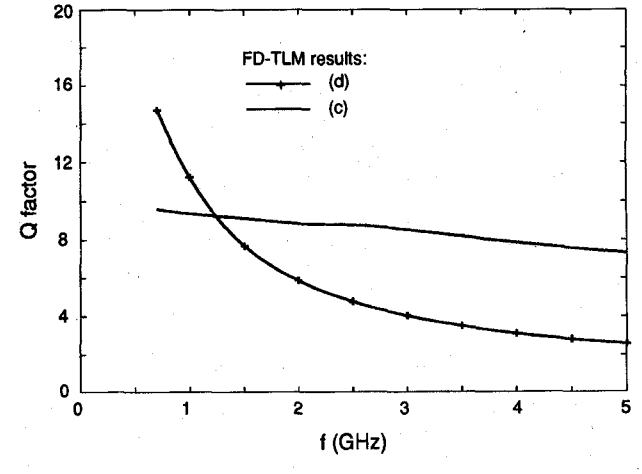

(c)

Fig. 7. Slow wave propagation characteristics of a bulk silicon MIS CPW with different doping widths, S. ($W = 40$ μm and $G = 25$ μm.) (a) Slow wave factbr versus frequency. (b) Attenuation versus frequency. (c) Quality factor versus frequency. Refer to Fig. 4 for structural details.

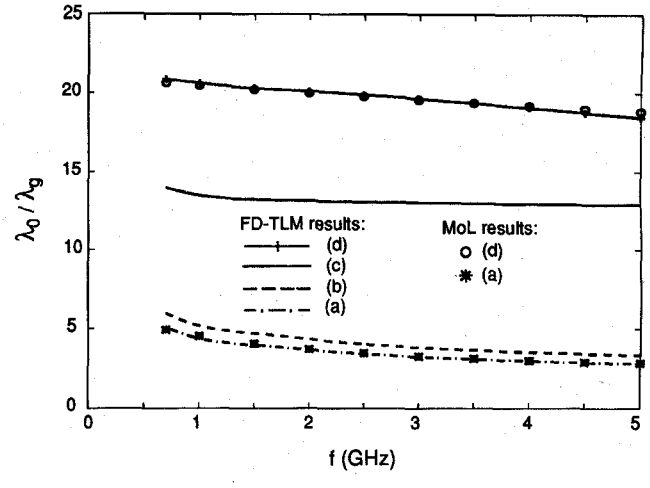

(a)

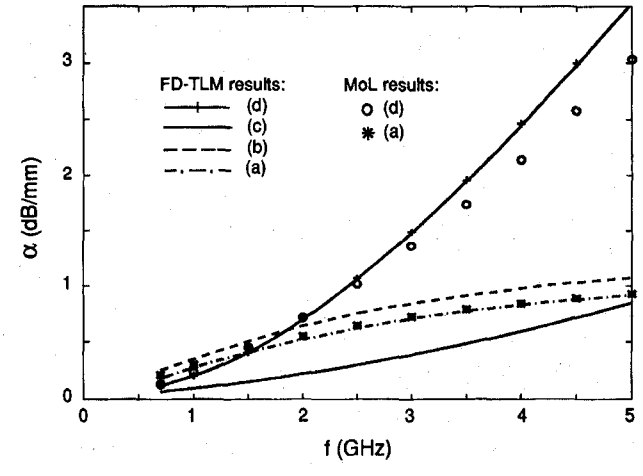

(b)

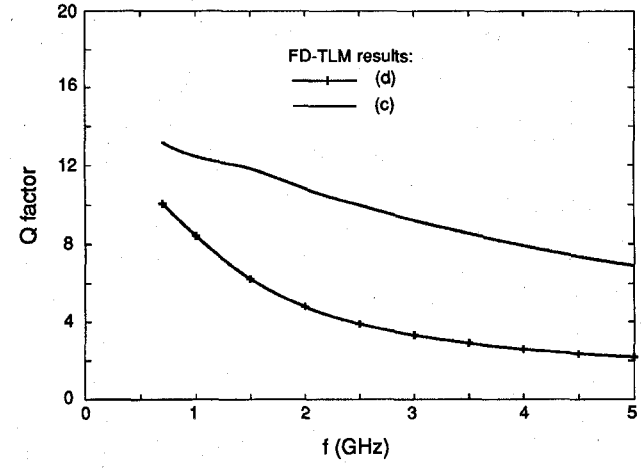

(c)

Fig. 8. Slow wave propagation characteristics of SOI MIS CPW with different doping widths, S ($W = 40$ μm and $G = 25$ μm.) (a) Slow wave factor versus frequency. (b) Attenuation versus frequency. (c) Quality factor versus frequency. Refer to Fig. 4 for structural details.

higher. The introduction of a lossless SiO_2 layer between the doping layer and the high-resistivity Si substrate plays an important role in confining the electric field in the insulating layer beneath the coplanar conductors. This may be the reason why SOI structures with selected B^{2+} ion-implantation doping exhibit reasonably large slow wave factors with little dispersion. The analysis indicates that the SOI structure with a lateral doping width as shown in Fig. 4(c) not only provides

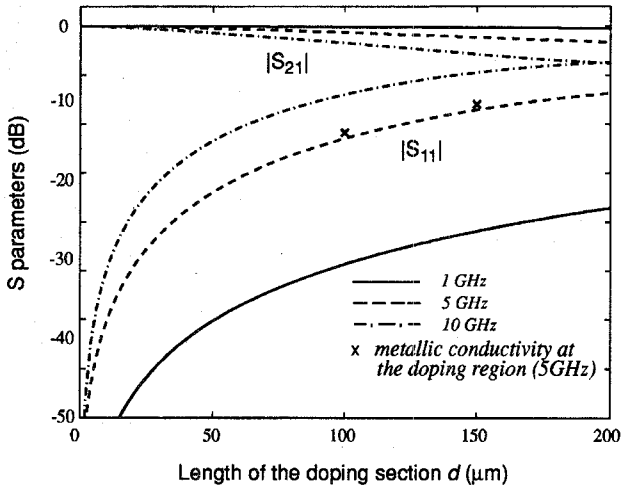

Fig. 9. S-parameters for the abrupt discontinuity between the undoped CPW and the MIS CPW versus the length of the doping section, d, at frequencies 1, 5, and 10 GHz ($S = W + 2G$, $W = 40$ μm, $G = 25$ μm, $t_o = 0.1$ mm, $t_{\text{sub}} = 525$ μm, $\epsilon_{ro} = 3.9$, and $\epsilon_r = 11.8$).

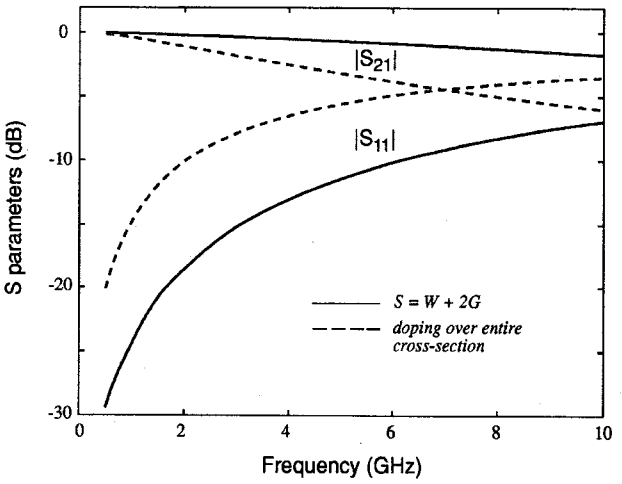

Fig. 10. S-parameters for the abrupt discontinuity between the undoped CPW and the MIS CPW with different lateral doping widths. (a) $S = W+2G$ and (b) *doping over entire cross section* ($d = 100$ μm, $W = 40$ μm, $G = 25$ μm, $t_o = 0.1$ μm, $t_{sub} = 525$ μm, $\epsilon_{ro} = 3.9$, and $\epsilon_r = 11.8$).

a better slow wave factor, but the Q-factor is also improved over that of the bulk structure.

B. S-Parameters for the Abrupt Transition Between the MIS CPW and a CPW on Undoped High-Resistivity Silicon

To illustrate the scattering effects introduced by the transition from an undoped to a doped substrate, we first investigate the structure in Fig. 5 with homogeneous conductor dimensions and a lateral doping width of $S = W+2G$. By increasing the frequency and the length of the doping region, Fig. 9 shows clearly that the transmission coefficient decreases significantly, and the reflection coefficient exhibits a strong dependency on both parameters. The sensitivity of S_{11} with respect to the length of the slow wave structure is due to some back reflection from the opposite transition. The effect of the frequency on S_{11} is most likely caused by the skin effect of the doping layer. At higher frequencies (>5 GHz) the electric field penetrates much less into the doping layer then at 1 GHz. At frequencies higher than 5 GHz, the doping layer appears like a groundplane separated by a 0.1 μm thick SiO_2 insulating layer. In this case, the electric field is mostly concentrated between the center conductor of the CPW and the doping layer rather than in the 25-μm wide slots between the center conductor and the uniplanar ground-plane. Hence, the characteristic impedance is not only very low, but the wave encounters a transition from a CPW mode into a microstrip-like mode, which introduces even higher reflections. This explanation is also supported by results from an analysis in which the conductivity of the doping layer is increased to that of a lossy conductor (cross-points in Fig. 9).

Fig. 10 illustrates a comparison between two types of lateral doping widths for the structure in Fig. 5—homogeneous doping over the entire transmission line cross section and doping only over the strip and both slot regions. The results clearly indicate that homogeneous doping over the entire cross section not only lowers the characteristic impedance of this CPW section and, thus, increases the reflection coefficient, but also increases the overall losses. This observation is in line with our previous conclusion that in order to achieve the lowest loss slow wave mode, doping over the whole cross section should be avoided. At the same time one would also achieve a lower reflection coefficient at the transition.

C. Laterally Doped MIS CPW with Double-Step Discontinuity

Fig. 11 illustrates S-parameters for an MIS CPW with a laterally confined doping region ($S = W + 2G$) and double-step discontinuity in the conductor and ground-plane (Fig. 6), as well as for various CPW discontinuities on a normal insulating substrate. The dimensions of the conductors on the insulating substrate are designed for 50 Ω. On the doped region, the characteristic impedance in this section drops to less than 5 Ω. The reflection coefficient of such a transition is shown in Fig. 11 curves (a) and (c). For comparison, curves (d), (e), and (b) represent transitions between 50 Ω–25 Ω–50 Ω, 50 Ω–10 Ω–50 Ω, and 50 Ω–50 Ω–50 Ω CPW transmission lines on the insulating substrate, respectively. Curves (a) and (c) seem to suggest that the impedance step is even more pronounced than what could be expected from a comparison with curve (e). This, however, is not the case. The larger reflection coefficient is due to the fact that, as discussed before in conjunction with Fig. 9, the doped region acts more like a groundplane to the CPW mode, evidently changing the CPW mode to a microstrip mode and, thus, representing a more pronounced discontinuity to the CPW mode-field incident into the discontinuity plane. As a final note, the reflection coefficient for curve (b) clearly indicates that, although both sides of the discontinuity are of 50 Ω, the change in the conductor dimensions still represent a discontinuity to the electromagnetic field and thus causing the reflection to occur.

IV. Conclusions

A numerical analysis of slow wave propagation, losses, and Q-factor in bulk silicon and SOI MIS CPW has been presented. The analysis is based on the FDTLM method. It was found that

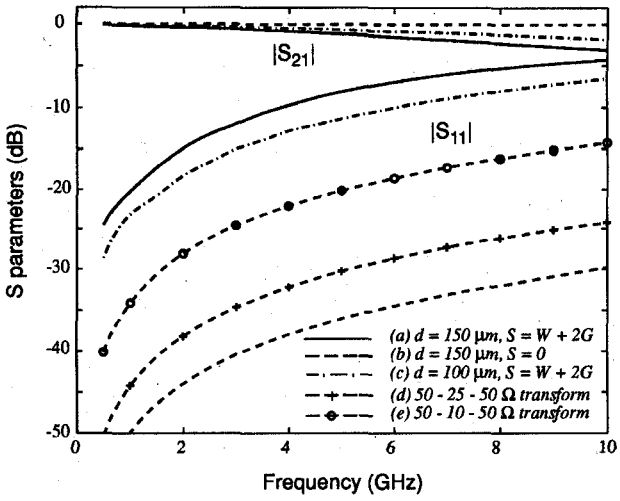

Fig. 11. S-parameters for the double-step discontinuity ($d = 100$ μm and 150 μm, $W = 40$ μm, $G = 25$ μm, $t_o = 0.1$ μm, $t_{sub} = 525$ μm, $\epsilon_{ro} = 3.9$, and $\epsilon_r = 11.8$).

large slowing factors at low losses can be achieved by optimizing the lateral extent of the semiconductor doping region. It was furthermore found that SOI structures show a better Q-factor with less dispersion than the bulk silicon structures. Scattering effects at abrupt transitions between MIS CPW and undoped CPW discontinuities have been investigated as well. It was found that the doping region not only introduces a very low characteristic impedance with a correspondingly high-reflection coefficient, but that the doping layer also acts as a lossy ground-plane in close vicinity to the center conductor of the CPW and, thus, obviously changes the CPW mode to a microstrip mode in that region. This change in field pattern introduces additional reflections that cannot be explained by only considering the impedance step between the doped and undoped CPW section.

ACKNOWLEDGMENT

The authors would like to thank Dr. M. Kim, Philips Laboratories, and North American Philips Corporation for helpful discussions and measurements.

REFERENCES

[1] H. Hasegawa and H. Olizaki, "MIS and Schottky slow wave coplanar striplines on GaAs substrates," *Electron. Lett.*, vol. 13, no. 22, pp. 663–664, Oct. 1977.

[2] Y. Fukuoka, Y. Shih, and T. Itoh, "Analysis of slow wave coplanar waveguide for monolithic integrated circuits," *IEEE Trans. Microwave Theory Tech.*, vol. MTT-31, no. 7, pp. 567–573, July 1983.

[3] R. Sorrentino, G. Leuzzi, and A. Silbermann, "Characteristics of metal-insulator-semiconductor coplanar waveguides for monolithic microwave circuits," *IEEE Trans. Microwave Theory Tech.*, vol. MTT-32, no. 4, pp. 410–415, Apr. 1984.

[4] C. Seguinot, P. Kennis, P. Pribetich, and J. P. Villotte, "MIS slow wave coplanar line: a comparison of theoretical and experimental characteristics," in *Proc. 16th European Microwave Conf.* Dublin Ireland, 1986, pp. 445–446.

[5] T. C. Mu, H. Ogawa, and T. Itoh, "Characteristics of multiconductor asymmetric slow wave microstrip transmission lines," *IEEE Trans. Microwave Theory Tech.*, vol. MTT-34, no. 12, pp. 1471–1477, Dec. 1986.

[6] Y. R. Kwon, V. M. Hietala, and K. S. Champlin, "Quasi-TEM analysis of slow wave mode propagation on coplanar microstructure MIS transmission lines," *IEEE Trans. Microwave Theory Tech.*, vol. MTT-35, no. 6, pp. 545–551, June 1987.

[7] K. Wu, "New prospective coplanar metal-insulator-semiconductor (MIS) monolithic structure," *Electron. Lett.*, vol. 24, no. 5, pp. 262–264, Mar. 1988.

[8] K. Wu and R. Vahldieck, "Propagation characteristics of MIS transmission lines with inhomogeneous doping profile," *IEEE Trans. Microwave Theory Tech.*, vol. 38, no. 12, pp. 1872–1878, Dec. 1990.

[9] ——, "Hybrid-mode analysis of homogeneously and inhomogeneously dope low-loss slow wave coplanar transmission lines," *IEEE Trans. Microwave Theory Tech.*, vol. 39, no. 8, pp. 1348–1360, Aug. 1991.

[10] J. W. Mayer, L. Eriksson, and J. A. Davies, *Ion Implantation in Semiconductors.* New York: Academic, 1970, ch. 2.

[11] H. Jin and R. Vahldieck, "The frequency-domain TLM method," in *1992 IEEE Int. Microwave Symp. Dig.*, pp. 775–778, June 1992.

[12] ——, "The frequency-domain transmission line matrix method—A new concept," *IEEE Trans. Microwave Theory Tech.*, vol. 40, no. 12, pp. 2207–2218, Dec. 1992.

[13] D. P. Johns, A. J. Wlodarczyk, A. Mallik, and C. Christopoulos, "New TLM technique for steady-state field solutions in three dimensions," *Electron. Lett.*, vol. 29, no. 18, pp. 1692–1694, 1992.

[14] J. Huang, R. Vahldieck, and H. Jin, "Fast frequency-domain TLM analysis of 3-D circuit discontinuities," in *Proc. 9th Annual Review Progress Applied Computational Electromagnetics Symp.*, 1993, pp. 475–481.

[15] H. Jin and R. Vahldieck, "Full-wave analysis of coplanar waveguide discontinuities using the frequency-domain TLM method," *IEEE Trans. Microwave Theory Tech.*, vol. 41, no. 9, pp. 1538–1542, Sept. 1993.

[16] J. Huang, "Frequency domain transmission line matrix method and its applications to electromagnetic analysis," Ph.D. dissertation, Univ. Victoria, Victoria, Canada, 1995.

[17] P. B. Johns and R. L. Beurle, "Numerical solution of 2-dimensional scattering problems using a transmission-line matrix," *Proc. Inst. Elect. Eng.*, vol. 118, no. 9, pp. 1203–1208, 1971.

[18] W. J. R. Hoefer, "The transmission line matrix method: Theory and applications," *IEEE Trans. Microwave Theory Tech.*, vol. MTT-33, pp. 882–893, Oct. 1985.

Shuoqi Chen received the B.Sc. degree in physics from Xiamen University, Xiamen, China, in 1982 and the M.Sc. degree in microwave electronic engineering from Nanjing Electronics Devices Institute, Nanjing, China, in 1988. Since 1993 he has received the Graduate Research Engineering and Technology (GREAT) Award scholarship from the Science Council of British Columbia, Canada, and is currently working toward the Ph.D. degree with the Department of Electrical and Computer Engineering at the University of Victoria, British Columbia, Canada.

From 1982 to 1985, he was an Engineer at Nanjing Electron Tubes Manufacturer, Nanjing, China, where he was involved in the development of microwave electron tubes and electrovacuum technology. From 1988 to 1990, he served as a Research Manager and R & D Engineer at Nanjing Electronics Devices Institute, Nanjing, China, where he was engaged in the design and development of microwave semiconductor components and GaAs power MMIC's. His research involves large-signal GaAs FET's modeling, broadband semiconductor laser diode modulation for fiber-optic communications, and numerical modeling of passive and active planar structures for MHMIC and MMIC applications. His current research interests are in the areas of numerical techniques for modeling electromagnetic fields and wave, computer-aided design of RF/microwave components and integrated circuits, semiconductor devices, and optoelectronics.

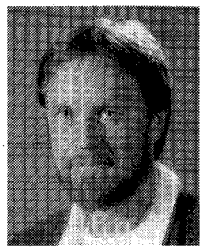

Rüdiger Vahldieck (M'85–SM'86) received the Dipl.Ing. and D.Ing. degrees in electrical engineering from the University of Bremen, West Germany, in 1980 and 1983, respectively.

From 1984 to 1986 he was a Research Associate at the University of Ottawa, Canada. In 1986 he joined the Department of Electrical and Computer Engineering at the University of Victoria, British Columbia, Canada. As of 1991 he is a Full Professor. During the Fall and Spring of 1992–1993 he was a Visiting Scientist at the Ferdinand-Braun-Institute für Hochfrequenztechnik in Berlin, Germany. His research interests include numerical methods to model electromagnetic fields for computer-aided design of microwave, millimeter-wave, and opto-electronic integrated circuits. In particular he is interested in the design aspects of passive and active components for MIC and MMIC applications, as well as the development of CAD tools for filter structures, multiplexers, and polarizers. Recently, he also became involved in the design and simulation of broadband fiber-optic communication systems and subsystems.

Together with three coauthors, he received the outstanding publication award of the Institution of Electrical and Radio Engineers in 1983. He has published more than 100 technical papers mainly in the field of microwave CAE. He is on the editorial board for the IEEE TRANSACTIONS ON MICROWAVE THEORY AND TECHNIQUES, and he has served on the Technical Program Committee of IEEE International Microwave Symposium since 1992.

Jifu Huang received the B.Eng. and M.Eng. degrees in radio engineering from Nanjing Institute of Technology (now Southeast University), Nanjing, China, in 1982 and 1987, respectively. From 1991 to 1994, he worked toward the Ph.D. degree with the Department of Electrical and Computer Engineering, University of Victoria, British Columbia, Canada.

He joined the Faculty of Engineering at Southeast University in 1982 where he worked as a Research and Teaching Assistant and as a lecturer from 1987 to 1991. Since April 1994, he has been a post-doctoral fellow at the Research Center for Advanced Microwave and Space Electronics, Ecole Polytechnique of Montreal, P.Q., Canada. His current research interest is in numerical modeling and CAD of microwave/millimeter-wave integrated circuits for communications.